Structural tuning of Quinoxaline-Benzodithiophene copolymers via alkyl side chain manipulation: Synthesis, Characterization and Photovoltaic Properties

Journal:	*Journal of Materials Chemistry A*
Manuscript ID:	TA-ART-03-2014-001479.R1
Article Type:	Paper
Date Submitted by the Author:	28-Apr-2014
Complete List of Authors:	Tessarolo, Marta; Consiglio Nazionale delle Ricerche (CNR), Istituto per lo Studio dei Materiali Nanostrutturati (ISMN) Gedefaw, Desta; Chalmers University of Technology, Department of Chemical and Biological Engineering, Polymer Technology Bolognesi, Margherita; Laboratory MIST E-R, Liscio, Fabiola; Consiglio Nazionale delle Ricerche (CNR), Istituto per la Microelettronica e Microsistemi (IMM) Henriksson, Patrik; Chalmers University of Technology, Department of Chemical and Biological Engineering, Polymer Technology Zhuang, Wenliu; Chalmers University of Technology, Department of Chemical and Biological Engineering, Polymer Technology Milita, Silvia; Consiglio Nazionale delle Ricerche (CNR), Istituto per la Microelettronica e Microsistemi (IMM) Muccini, Michele; Consiglio Nazionale delle Ricerche (CNR), Istituto per lo Studio dei Materiali Nanostrutturati (ISMN) Wang, Ergang; Chalmers University of Technology, Department of Chemical and Biological Engineering, Polymer Technology Seri, Mirko; Consiglio Nazionale delle Ricerche (CNR), Istituto per la Sintesi Organica e la Fotoreattività (ISOF) Andersson, Mats R; Chalmers University of Technology, Dept. of Organic Chemistry and Polymer Technology

Journal of Materials Chemistry A

ARTICLE TYPE

Structural tuning of Quinoxaline-Benzodithiophene copolymers *via* alkyl side chain manipulation: Synthesis, Characterization and Photovoltaic Properties

Marta Tessarolo,[a] Desta Gedefaw,*[b] Margherita Bolognesi,[c] Fabiola Liscio,[d] Patrik Henriksson,[b] Wenliu

5 Zhuang,[b] Silvia Milita,[d] Michele Muccini,[a] Ergang Wang,[b] Mirko Seri*[e] and Mats R. Andersson*[b,f].

We report here the synthesis and characterization of two novel semiconducting quinoxaline (FQ)-benzodithiophene (BDT) based copolymers, PFQBDT-TR$_1$ and PFQBDT-T2R$_2$, in which the BDT unit is
10 substituted with either 2-octylthienyl (-TR$_1$) or 2,3- dihexylthienyl (-T2R$_2$), respectively, as side groups. The effect of the alkyl side chain(s), linked to the thienyl side groups, on optical, electronic and morphological properties of the resulting polymers is investigated and correlated with the photovoltaic performance. Solution-processed BHJ solar cells, using these copolymers as electron donor materials and PC$_{61}$BM (or PC$_{71}$BM) as electron acceptor counterpart, are prepared by blade-coating technique in
15 ambient conditions. As a result, power conversion efficiencies (PCEs) of ~ 5.7 % and ~ 3.4 % have been achieved for PFQBDT-TR$_1$ and PFQBDT-T2R$_2$ based devices, respectively, highlighting the crucial role of the alkyl portion of the π-conjugated side segment on the optoelectronic properties of this class of copolymers.

1 Introduction

20 Solution-processed organic solar cells represent the newest generation of technologies in solar power generation, offering benefits in terms of low manufacturing costs, large area coverage, compatibility with flexible and light-weight substrates, earth-abundant constituents and architectural tunability over multiple
25 length scales.[1] π-conjugated polymers and fullerene derivatives are the typical constituents of the active layer in so-called bulk heterojunction (BHJ) organic solar cells[2], in which these two materials, acting as an electron donor and an electron acceptor, respectively, are deposited as a finely intermixed blend film
30 placed between a semitransparent anode (ITO) and a metal cathode. The power conversion efficiency (PCE) of lab-scale single-junction BHJ solar cells has reached ~ 8-10 %[3] by the synergic development of novel active materials,[3,4] enhanced understanding of polymeric film microstructure[5] and meticulous
35 device optimization,[6] indicating a bright future for organic photovoltaic (OPV) cells in commercial applications.[7]

The properties of photoactive materials are one of the most determining factors for the preparation of highly efficient polymer solar cells.[8] An ideal donor polymer should fulfill some
40 fundamental requirements such as: *i*) broad absorption spectrum with high absorption coefficient, *ii*) high charge carrier mobility, *iii*) optimal energetic alignment of the HOMO and LUMO energy

levels with those of the acceptor material to ideally provide large open-circuit voltages (V$_{OC}$), environmental stability and efficient
45 exciton dissociation,[9] and *iv*) appropriate film forming and nano-structuring capability once blended with the acceptor counterpart.

A well-known strategy to obtain efficient donor polymers, is to alternate electron-rich and electron-deficient conjugated moieties in the backbone. In this *push–pull* architecture, the nature and the
50 electronic properties of the donor and acceptor units as well as the substituents anchored to the building blocks, play a fundamental role and represents an important and widely spread technique used to modulate the chemical and physical properties of the resulting semiconducting polymers. Indeed, besides the
55 design of conjugated polymers with different backbone structures, the modulation of the polymers' properties by changing the influence of the electronic distribution, the geometry, number and position of their side groups has also attracted much attention as molecular design motif for
60 photoactive polymers.[10]

Among these, two-dimensional (2-D) π-conjugated polymers exhibited several advantages and very promising OPV responses. The use of alkyl substituted aromatic side groups on the copolymer backbone has been demonstrated to both enhance the
65 solubility of the macromolecule and contribute to extend the π-conjugation from the backbone to the lateral substituents, leading to a more extended or 2D π-conjugated systems.[11] For instance, Li *et al.*[11a] reported the synthesis and characterization of a 2D-

conjugated polymer with alkyl-thiophene π-conjugated side chains, which showed improved optical, electronic and electrical properties with enhanced photovoltaic responses (PCEs of $\sim$ 6 %) compared the corresponding alkoxy-substituted copolymer.

Recently, we also designed new 2D-conjugated *push-pull* polymers P(1)-Q-BDT-4TR and P(2)-FQ-BDT-4TR,[12] based on alternate alkyl-dithiophene (2TR) substituted benzo[1,2-b:4,5-b']dithiophene (BDT) and quinoxaline (Q) units. We found that the introduction of dithiophene-based (2TR) side chains on the BDT unit effectively allows to obtain a polymer with red-shifted absorption maxima ($\Delta_{\lambda max}$ > 30 nm), lowered HOMO level (Δ_{HOMO} > 0.1 eV), with respect to the analogous polymer (PBDT–TFQ)[13] containing alkoxy side chains on the BDT unit. As a result, BHJ solar cells with short-circuit current density (J_{SC}), open-circuit voltage (V_{OC}), fill factor (FF) and PCE of 10.2 mA/cm^2, 0.90 V, 58 % and 5.3%, respectively, were prepared.

Besides extending the lateral π-conjugation of 2D-polymers, the nature, length, conformation (linear or branched), position and number of alkyl side chains in the side groups strongly influence the main properties of the resulting polymers, such as: *i*) solubility, *ii*) miscibility with the acceptor counterpart and, *iii*) structural conformation by favoring planarity or torsion angles on the backbone, thus promoting or hindering *intra-* and *inter-*molecular interactions.[14] As a result, the optical, morphological and electrical properties of the polymer films can be controlled and optimized. Indeed, the fine structural tuning of alkyl side chains represents an effective and common design strategy for various classes of efficient donor polymers.

In this work, we report the synthesis and characterization of two novel *p*-type BDT-quinoxaline based *push-pull* polymers, PFQBDT-TR$_1$ and PFQBDT-T2R$_2$ (Figure 1), in which the BDT core unit was substituted with either 2-octylthienyl (-TR$_1$) or 2,3-dihexylthienyl (-T2R$_2$), respectively, as side groups. Since the polymers have similar molecular structures, the comparison between them will provide useful information on the influence of the alkyl side chain(s) of the 2D-conjugated structure on the resulting optical, morphological and electrical properties. Solution-processed BHJ solar cells, using PFQBDT-TR$_1$ and PFQBDT-T2R$_2$ as electron donor materials and PC$_{61}$BM (or PC$_{71}$BM) as electron acceptor counterpart, were fabricated in air by blade-coating technique. PCEs of $\sim$ 5.7 % and $\sim$ 3.4 % have been achieved for PFQBDT-TR$_1$:PC$_{61}$BM and PFQBDT-T2R$_2$:PC$_{61}$BM based devices, respectively, highlighting how the architecture of the alkyl portion of the π-conjugated side segment (thiophene ring) plays a determining role in polymer self-assembly in thin-films and can influence the resulting optoelectronic properties of these BDT-quinoxaline based copolymers.

2 Experimental Section

2.1 General remarks

5,8-bis(5-bromothiophen-2-yl)-6,7-difluoro-2,3-bis(3-(octyloxy)phenyl)quinoxaline (7) was prepared according to previously reported procedures.[11g-12] Tetrahydrofuran (THF) was dried over Na/benzophenone and freshly distilled prior to use. Other reagents and solvents were commercial grade and used as received without further purification. ^{1}H NMR and ^{13}C NMR

spectra were acquired from a Varian Inova 400 MHz NMR spectrometer. Tetramethylsilane was used as an internal reference with deuterated chloroform as solvent. Size exclusion chromatography (SEC) was performed on Waters Alliance GPCV2000 with a refractive index detector, with columns: Waters Styragel® HT 6E×1, Waters Styragel® HMW 6E×2. The eluent was 1,2,4-trichlorobenzene, the working temperature was 135 °C, and the dissolution time was 2 hours. The concentration of the samples was 0.5 mg/mL, which was filtered (filter: 0.45 μm) prior to the analysis. The relative molecular masses were calculated by calibration relative to polystyrene standards. Ultraviolet–visible (UV–vis) absorption spectra were measured with a PerkinElmer Lambda 900 UV–vis–NIR absorption spectrometer.

Square-wave voltammetry (SWV) measurements were carried out on a CH-Instruments 650A Electrochemical Workstation. A three-electrode setup was used with platinum wires both as working electrode and counter electrode, and Ag/Ag$^+$ used as reference electrode calibrated with Fc/Fc$^+$. A 0.1 M solution of tetrabutylammoniumhexafluorophosphate (Bu$_4$NPF$_6$) in anhydrous acetonitrile was used as supporting electrolyte. The polymers were deposited onto the working electrode from chloroform solution. In order to remove oxygen from the electrolyte, the system was bubbled with nitrogen prior to each experiment. The nitrogen inlet was then moved above the liquid surface and left there during the scans. HOMO and LUMO levels were deduced from their respective ionization potentials and electron affinities, estimated from peak potentials of the third scan by setting the oxidative peak potential of Fc/Fc$^+$ *vs.* the normal hydrogen electrode (NHE) to 0.63 V and the NHE *vs.* the vacuum level to 4.5 V.[15]

2.2 OPV Device fabrication and characterization

All materials, PEDOT:PSS (poly(3,4-ethylenedioxythiophene): poly(4-styrenesulfonate), Clevios P VP A1 4083, H.C. Starck), PC$_{61}$BM ([6,6]- phenyl-C61-butyric acid methyl ester, Solenne BV) (or PC$_{71}$BM) and various anhydrous solvents (Sigma-Aldrich) were purchased from commercial sources and used without further purification. Patterned ITO-coated glasses (Rs $\sim$ 10 Ω/□) were cleaned in sequential sonicating baths (for 15 min) of deionized water, acetone and isopropanol. After the final sonication step, substrates were dried with a stream of N$_2$ gas and then placed in an oxygen plasma chamber for 10 min. Next, a thin layer ($\sim$ 30 nm) of PEDOT:PSS was spun-cast on the ITO surface and subsequently annealed at 150 °C for 15 min. The active layer blend solutions were formulated inside the glove box and stirred overnight at 80°C. For optimized devices, a total concentration of 30 mg/mL in *o*-dichlorobenzene (ODCB) was used for both donors. The blend solutions were deposited in ambient conditions by blade-coating on top of the ITO/PEDOT:PSS surface. Before cathode deposition, the substrates were then either thermally annealed or left as-cast. To complete the device fabrication, LiF and Al (0.6 nm and 100 nm) were deposited sequentially without breaking vacuum ($\sim$3 × 10^{-6} Torr) using a thermal evaporator directly connected to the glove box. The current–voltage (*I–V*) characteristics of all OPV devices were recorded by a Keithley 236 source-measure unit under simulated AM1.5G illumination of 100 mW/cm^2 (Abet Technologies Sun 2000 Solar Simulator). The light intensity was determined by a calibrated silicon solar

cell fitted with a KG5 color glass filter to bring spectral mismatch to unity. The active area of the solar cell was exactly 6 mm^2. During testing, each cell was carefully masked, by calibrated mask, to prevent an excess photocurrent generated from the parasitic device regions outside the overlapped electrodes area. All solar cells were tested inside the glove box in oxygen and moisture free environment. External Quantum Efficiency (EQE) was measured outside the glove-box with a home-built system on encapsulated devices. Monochromatic light was obtained with a Xenon arc lamp from Lot-Oriel (300 Watt power) coupled with a Spectra-Pro monochromator. The photocurrent produced by the device passed through a calibrated resistance (50 Ω) and the voltage drop signal was collected through the resistance with a Lock-In Digital Amplifier-SR830. Signal was pulsed by means of an optical chopper (~ 300 Hz frequency). A calibrated silicon photodiode was used as reference.

2.3 Thin-film characterization

All thin-film characterizations were performed in air. Solution and film optical absorption spectra were recorded on a JASCO V-550 spectrophotometer. The thickness of the various films was measured by a profilometer (KLA Tencor, P-6). All active films were characterized on glass/ITO/PEDOT:PSS substrates and subsequently corrected for the background signal, in order to reproduce the effective condition and the real nanomorphology of the active layer. Atomic Force Microscopy (AFM) images were taken with a Solver Pro (NT-934 MDT) scanning probe microscope in tapping mode. The AFM images were recorded directly on tested devices.

The crystallinity of PFQBDT-TR$_1$ and PFQBDT-T2R$_2$ films was investigated by Grazing Incidence X-Ray Diffraction (GIXRD) measurements performed at the ELETTRA-XRD1 beamline at Trieste's synchrotron facility (Italy) using a monochromatic beam with a wavelength (λ) of 1 Å and a dimension of 0.2×0.2 (H×V) mm^2. The incident angle of the X-ray beam, α$_i$, was chosen slightly larger than the critical angle for total reflection of the organic film (~0.12°), in order to penetrate through the full film depth. The diffraction patterns were recorded using a 2D camera (Pilatus detector) placed normal to the incident beam direction. The PFQBDT-TR$_1$ and PFQBDT-T2R$_2$ films, characterized by GIXRD, were prepared by blade-coating semiconductor solutions in ODCB (15 and 10 mg/mL, respectively) on pre-cleaned and Si/SiO$_2$ substrates. The thickness of the resulting films were estimated to be ~ 180 nm for PFQBDT-TR$_1$ and ~ 100 nm for PFQBDT-T2R$_2$.

The hole mobility of the photosensitive layers was measured by the space charge limited current (SCLC)[16] method using devices with structure: glass/ITO/PEDOT:PSS/polymer:PC$_{61}$BM/Au. The processing conditions used for the active layers were the optimized ones. Charge mobility was extracted by fitting the current density–voltage curves, recorded in dark conditions, to the Mott–Gurney equation.

3 Results and Discussion

3.1 Synthesis of monomers and polymers

Polymers PFQBDT-TR$_1$ and PFQBDT-T2R$_2$ are shown in Figure 1 and were synthesized as reported in Scheme 1. 5,8-bis(5-bromothiophen-2-yl)-6,7-difluoro-2,3-bis(3-(octyloxy)phenyl)quinoxaline (**7**) was prepared according to previously reported procedures,[11g-12] while the other comonomers were synthesized, purified and characterized as described in ESI.
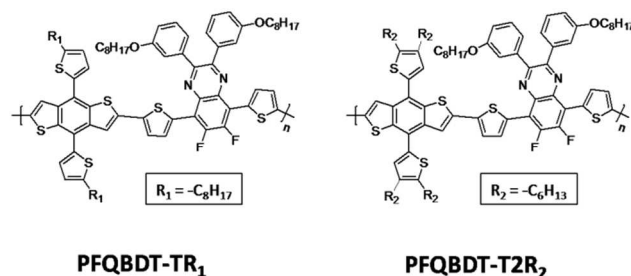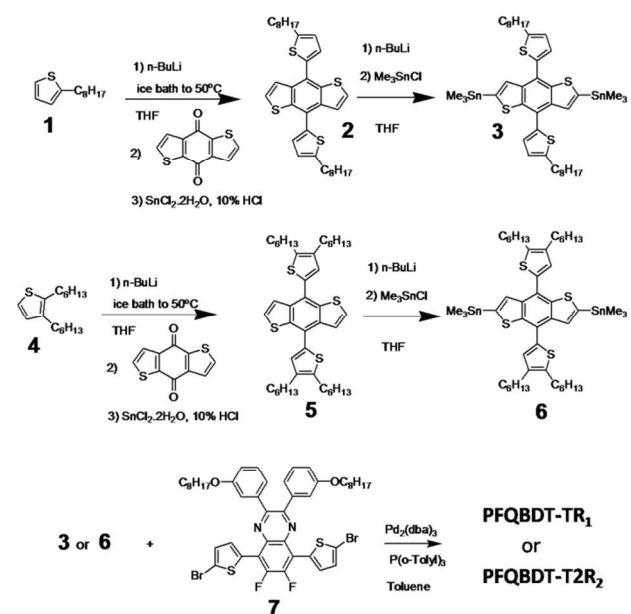

Figure 1. Chemical structures of polymers PFQBDT-TR$_1$ and PFQBDT-T2R$_2$.

Briefly, the BDT monomers ((4,8-bis(5-octylthiophen-2-yl)benzo[1,2-b:4,5-b']dithiophene-2,6-diyl)bis(trimethylstannane) (**3**) and (4,8-bis(4,5-dihexylthiophen-2-yl)benzo[1,2-b:4,5-b']dithiophene-2,6-diyl)bis(trimethylstannane) (**6**) were synthesized following the reaction sequences shown in Scheme 1.

Scheme 1. Synthetic route to alkyl-thiophene substituted BDT comonomers (3 and 6) and PFQBDT-TR$_1$ and PFQBDT-T2R$_2$ polymers.

2-Octylthiophene (**1**) or 2,3-dihexyl thiophene (**4**) was lithiated with *n*-BuLi to which benzo[1,2-b:4,5-b']dithiophene-4,8-dione was added and the intermediate compounds formed were reduced with SnCl$_2$.2H$_2$O in 10% HCl to afford compound **2** and **5** with 65% yield. The distannylated BDT monomers **3** and **6** were obtained from compound **2** and **5** by a step wise reaction that involves lithiation by *n*-butyllithium followed by quenching with trimethyltin chloride of the lithiated species. Monomer **3** was purified by recrystallization from isopropanol-THF mixture while compound **6** was purified by recrystallization from ethanol and isopropanol.

Polymers PFQBDT-TR$_1$ and PFQBDT-T2R$_2$ were

synthesized[12] via Stille cross-coupling reaction in toluene using tris(dibenzylideneacetone)-dipalladium(0) (Pd$_2$(dba)$_3$) and tri(o-tolyl)phosphine P(o-Tolyl)$_3$ as the catalyst[11g-12]. The resulting polymers were precipitated in methanol, collected by filtration and purified by Soxhlet extraction, using different organic solvents, to remove impurities and/or low molecular weight fractions. The remaining part was extracted with chloroform. The purified polymers exhibit comparable molar masses (M$_N$ and M$_W$), determined by high temperature GPC, as summarized in Table 1. In addition, both polymers exhibit good solubility in chlorinated solvents for device fabrication (e.g., $\geq$ 10 mg/mL in ODCB) thanks to the presence of several alkyl side chains linked to the different structural units.

3.2 Optical, electrochemical and nanostructural properties of polymers

The optical absorption spectra of the pristine polymers PFQBDT-TR$_1$ and PFQBDT-T2R$_2$ in dilute chloroform solutions and as thin-films are displayed in Figure 2. The detailed absorption data, including absorption maxima in solution and film as well as the corresponding onset and bandgap values are summarized in Table 1. In general, the polymers exhibit relatively broad absorption spectra, which indicates that a significant part of the solar spectral flux is absorbed, contributing to photocurrent generation.
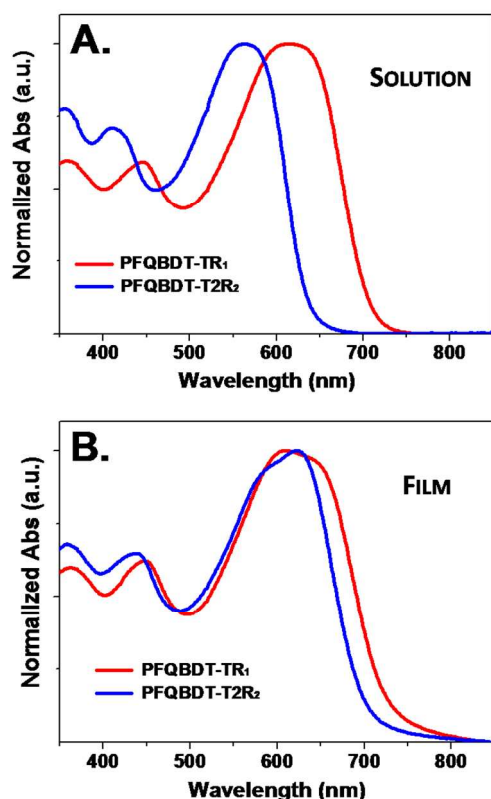

Figure 2. UV-Vis absorption spectra, normalized on the absorption maxima, of pristine polymers in: A) dilute ODCB solutions and, B) thin-films (deposited on glass from ODCB solution).

Both materials exhibit high energy absorption bands due to π-π* transition with a low-energy band arising from the intramolecular charge-transfer-like interactions, between the donor (BDT) and acceptor (FQ) moieties,[17] and from the intermolecular interactions between the polymer chains. However, the significantly different absorption profiles (Figure 2) of PFQBDT-TR$_1$ and PFQBDT-T2R$_2$, despite their similar molecular structure, suggest a strong influence of the alkyl side chains on the *intra-* and *inter-*molecular interactions, both in solution and solid state.

In the solution absorption spectra of polymers PFQBDT-TR$_1$ and PFQBDT-T2R$_2$ (Figure 2A) an evident red shift (by 52 nm) of the λ_{max} of PFQBDT-TR$_1$ versus that of PFQBDT-T2R$_2$ is observed (615 nm versus 563 nm, respectively). On the other hand, very similar λ_{max} are observed in the solid state spectra of the two polymers (Figure 2B), due to their different spectral shapes, indicating a different aggregation behavior (*vide infra*). In particular, a broader spectrum is registered for PFQBDT-TR$_1$ compared to PFQBDT-T2R$_2$, in the longer wavelength region ($\sim$700 nm). As a result, the absorption onset values (λ_{onset}) for PFQBDT-TR$_1$ and PFQBDT-T2R$_2$ films are $\sim$ 730 nm and 700 nm, from which the resulting optical gap (E$_{gap}^{opt}$) are estimated to be $\sim$ 1.70 and 1.77 eV, respectively.

The thin-film spectra of PFQBDT-TR$_1$ and PFQBDT-T2R$_2$ are significantly broadened and red-shifted relative to the solution spectra. Considering the absorption onsets (λ_{onset}), the resulting red shift magnitude ($\Delta\lambda_{onset} = \lambda_{onset}^{film} - \lambda_{onset}^{sol}$) drastically increases proceeding from PFQBDT-TR$_1$ to PFQBDT-T2R$_2$ ($\Delta\lambda_{onset}$ = 16 nm and 62 nm, respectively), likely due to enhanced *intra-* and *inter-*molecular interactions as a function of the alkyl side substitution on the thiophene rings.[18, 14d]

As shown in Figure 1, PFQBDT-TR$_1$ has linear octyl (-C$_8$H$_{17}$) side chains linked to the thiophene side group which play a role in improving the solubility of the polymer, without determining a significant steric hindrance or side chain congestion with the adjacent octyloxy (-OC$_8$H$_{17}$) substituent of the quinoxaline unit. As a consequence, we can assume that PFQBDT-TR$_1$ adopts a more favorable planar conformation, which could be responsible for a partial pre-aggregation of the polymer backbone in solution, in agreement with the relatively small $\Delta\lambda_{onset}$ for PFQBDT-TR$_1$ (16 nm) passing from solution to thin-film.

Diversely, in PFQBDT-T2R$_2$ the two *n*-hexyl side chains linked to the thiophene side groups could sterically interact with the adjacent octyloxy (-OC$_8$H$_{17}$) chains of the quinoxaline units. In order to minimize the side chain congestion and thus the conformational energy of the polymer backbone, we can suppose that PFQBDT-T2R$_2$ adopts a conformation where the side chains are placed away from each other, probably determining a partial twisting of the polymer backbone. This twisting, as expected, is stronger in solution, where the intermolecular interactions are relatively low, while in solid state the polymer chains will be forced to adopt a more planar conformation, similarly to the analogous derivative PFQBDT-TR$_1$. As a result, the partial planarization of the PFQBDT-T2R$_2$ backbone in thin-film, induced by the stronger π-π interchain interactions, is reflected in a drastically red-shifted onset ($\Delta\lambda_{onset}$ = 62 nm).

Note that, despite the aggregation tendency of both polymers, thus resulting in a similar behavior in solid state, they still exhibit different film absorption spectra ($\lambda_{onset\ (PFQBDT-TR1)}$ - $\lambda_{onset\ (PFQBDT-T2R2)}$ = 30 nm), suggesting a different self-organization of the

polymer chains, as supported by additional morphological and electrical investigations of PFQBDT-TR$_1$ and PFQBDT-T2R$_2$ based films.

To gain deeper insight into the molecular packing within the polymer films, 2D-GIXD images were collected on PFQBDT-TR$_1$ and PFQBDT-T2R$_2$ films and reported in Figures 3A and 3B, respectively. Both of them show a broad peak along the out-of-plane direction (q$_z$ lying in the 1.6-1.7 Å^{-1} range), corresponding to the π-stacking reflection (010) which suggests an orientation of the polymer backbone parallel to the substrate.
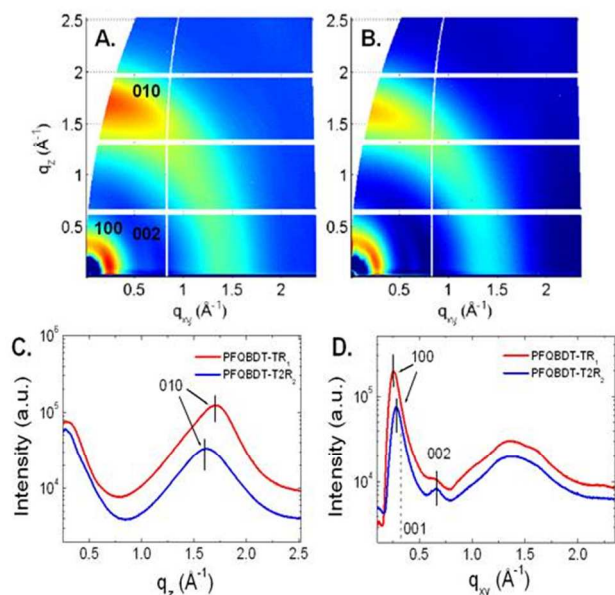

Figure 3. 2D-GIXRD images of (A) PFQBDT-TR1 and (B) PFQBDT-T2R2 films. All images have the same intensity log-scale. Scattering intensity integrated along (C) the Yoneda and (D) the specular direction (qxy ~ 0).

This "face-on" orientation is beneficial for the charge transport in the OPV device, and the effect is enhanced by reducing the $\pi-\pi$ stacking distance (d_{010}) between the backbones.[19] Interestingly, the distance d_{010}, extracted from the out-of-plane scattering intensity profile (Figure 3C), is ~ 3.7 Å and ~ 3.9 Å for PFQBDT-TR$_1$ and PFQBDT-T2R$_2$, respectively, confirming a

more cohesive solid-state molecular packing for PFQBDT-TR$_1$ polymer in agreement with the red-shifted absorption profile, enhanced charge mobility and photovoltaic properties. Moreover, the (010) peak intensity coming from PFQBDT-TR$_1$ film (normalized for the thickness) is higher than the other one, indicating a larger amount of crystalline domains for PFQBDT-TR$_1$.

The in-plane scattering intensity profiles, reported in Figure 3D, show two Bragg peaks at $q_{xy} \sim 0.26$ Å^{-1} and $q_{xy} \sim 0.66$ Å^{-1} for both polymers. Since the unit cells of these polymers are not know, peaks were index-linked on the base of polymer dimensions. The first peak, labeled as (100), is related with the distance of the lamellar spacing (d_{100}) along in the plane direction, which depends on the side chains packing, and it is slightly smaller for the hexyl (R$_2$) derivative PFQBDT-T2R$_2$ ($d_{ls} = \sim 22.0$ Å) than for the octyl (R$_1$) analogous PFQBDT-TR$_1$ ($d_{ls} = \sim 24.5$ Å). The second in-plane Bragg peak (002) corresponds to a distance of ~ 9.7 Å, which is in agreement with the half value of chain backbone repeat distance calculated using ChemBio3. The (001) should be hidden from (100) peak.

SWV was employed to examine the electrochemical properties and estimate the HOMO and LUMO energy levels of the polymers from the oxidation and reduction peak values (Figure S1), respectively. The resulting values are summarized in Table 1. The HOMO and LUMO energy levels of PFQBDT-TR$_1$ were estimated to be - 5.89 and - 3.61 eV, respectively, while those of PFQBDT-T2R$_2$ are - 5.87 and - 3.63 eV, respectively. The deep HOMO energies of both polymers suggest that high V$_{OC}$ should be achievable when PFQBDT-TR$_1$ and PFQBDT-T2R$_2$ are combined with PC$_{61}$BM or PC$_{71}$BM in BHJ OPV devices, according to the difference E(LUMO$_{ACCEPTOR}$) – E(HOMO$_{DONOR}$).[9b,c] In addition, the electrochemically derived HOMO energies are in an ideal range to ensure a good air stability of the polymers.[20, 9a] Considering that the LUMO level of the typical electron acceptors PC$_{61}$BM and PC$_{71}$BM are located at - 4.03 and - 4.13 eV respectively,[21] the LUMO offset between the donor and acceptor (ΔE_{LUMO}: E(LUMO$_{DONOR}$) – E(LUMO$_{ACCEPTOR}$)) should provide the driving force for an efficient exciton dissociation.[22] Finally, it should be reminded that no significant difference in the electrochemically determined HOMO and LUMO energy levels, thus in the resulting energy gap, was seen for the two polymers, likely due to the low sensitivity of this technique to the aggregation effects.[18]

Table 1. Molecular weights, optical, and electrochemical properties of PFQBDT-TR$_1$ and PFQBDT-T2R$_2$.

Polymer	M_n^a [kDa]	M_w^a [kDa]	Solution			Thin-film			E_{HOMO} [eV]	E_{LUMO} [eV]
			λ_{max} [nm]	λ_{onset} [nm]	$E_{gap}^{opt\ b}$ [eV]	λ_{max} [nm]	λ_{onset} [nm]	$E_{gap}^{opt\ b}$ [eV]		
PFQBDT-TR$_1$	25	64	615	714	1.74	610	730	1.70	-5.89	-3.61
PFQBDT-T2R$_2$	30	66	563	640	1.93	623	700	1.77	-5.87	-3.63

a) Determined by GPC relative to polystyrene standards using 1,2,4-trichlorobenzene as eluent. *b)* $E_{gap}^{opt} = 1240 / \lambda_{onset}$

Table 2. OPV characteristics of the most representative donor:PC$_{61}$BM based BHJ solar cells. The results reported are averaged over 6 cells.

Donor : PC$_{61}$BM ratio [wt/wt][a]	Thickness [nm]	DIO [% v/v]	Annealing[b] [°C]	J$_{SC}$ [mA/cm^2]	V$_{OC}$ [V]	FF [%]	PCE [%]
PFQBDT-TR$_1$: PC$_{61}$BM (2:1)	105	-	-	7.7	0.78	39	2.3
PFQBDT-TR$_1$: PC$_{61}$BM (2:1)	105	-	110	6.1	0.76	37	1.7
PFQBDT-TR$_1$: PC$_{61}$BM (1:1)	110	-	-	11.1	0.84	61	5.7
PFQBDT-TR$_1$: PC$_{61}$BM (1:1)	110	-	110	10.7	0.81	63	5.6
PFQBDT-TR$_1$: PC$_{61}$BM (1:1)	115	3%	-	8.8	0.74	48	3.2
PFQBDT-TR$_1$: PC$_{61}$BM (1:2)	120	-	-	8.9	0.79	67	4.7
PFQBDT-TR$_1$: PC$_{61}$BM (1:2)	120	-	110	8.1	0.79	64	4.1
PFQBDT-T2R$_2$: PC$_{61}$BM (2:1)	80	-	-	3.6	0.98	28	1.0
PFQBDT-T2R$_2$: PC$_{61}$BM (2:1)	80	-	110	3.1	0.97	30	0.9
PFQBDT-T2R$_2$: PC$_{61}$BM (1:1)	80	-	-	6.8	0.99	43	2.9
PFQBDT-T2R$_2$: PC$_{61}$BM (1:1)	80	-	110	6.9	0.96	47	3.1
PFQBDT-T2R$_2$: PC$_{61}$BM (1:2)	65	-	-	6.3	0.99	49	3.1
PFQBDT-T2R$_2$: PC$_{61}$BM (1:2)	65	-	110	6.5	0.96	54	3.4
PFQBDT-T2R$_2$: PC$_{61}$BM (1:2)	75	3%	110	6.2	0.94	53	3.1

a) Active layers from ODCB solutions; *b)* Annealing time: 10 min.

3.3 Photovoltaic properties and thin-film characterization

In order to investigate the impact of the alkyl side chains on the photovoltaic properties of PFQBDT-TR$_1$ and PFQBDT-T2R$_2$, we prepared BHJ solar cells using PC$_{61}$BM (or PC$_{71}$BM) as acceptor (A) counterpart. A conventional device configuration, glass/ITO/PEDOT:PSS/Active Layer/LiF/Al, was employed. The active blends were deposited by blade-coating in air from dry ODCB solutions, and notably the most efficient OPV solar cell was produced without the need of processing solvent additives. Further details for the device fabrication and characterization are given in the Experimental Section. Table 2 and Table S1 summarize the photovoltaic response data including V$_{OC}$, J$_{SC}$, FF and PCE. The OPV responses of PFQBDT-TR$_1$ and PFQBDT-T2R$_2$ based solar cells are dependent on the blend composition, since the tuning of the D:A blend ratio is pivotal to reach the best compromise between the light harvesting, charge carrier transport as well as ideal morphology in the bulk heterojunction, thus minimizing the loss mechanisms.[23] The optimal D:A ratio was found to be 1:1 (wt/wt) for PFQBDT-TR$_1$ and 1:2 (wt/wt) for PFQBDT-T2R$_2$. Upon increasing or decreasing the donor content in the active blends, a significant drop in J$_{SC}$, V$_{OC}$, or FF was observed, resulting in lower PCEs. Several unsuccessful attempts to optimize the OPV performance of the devices were carried out, for instance by using different annealing temperature and time, processing solvent additive (1,8-diiodooctane, DIO) and PC$_{71}$BM as alternative acceptor (Table 2 and S1).

OPV current density-voltage (J-V) plots, under standard illumination, for the most efficient solar cells based on PFQBDT-TR$_1$:PC$_{61}$BM and PFQBDT-T2R$_2$:PC$_{61}$BM (D:A wt/wt ratio of 1:1 and 1:2, respectively) active blends are shown in Figure 4.
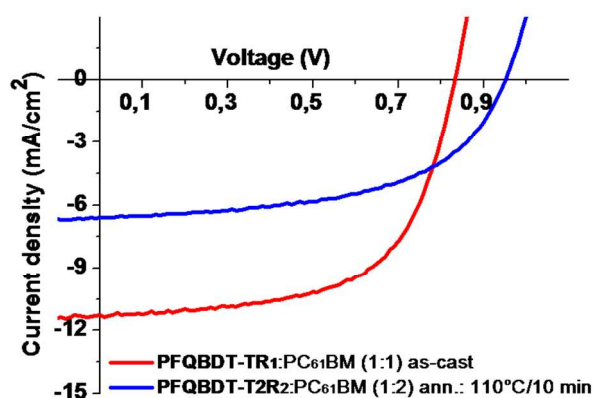

Figure 4. *J-V* plot, under standard illumination, of the best performing solar cells based on as-cast 1:1 (wt/wt) PFQBDT-TR$_1$:PC$_{61}$BM (red) and annealed 1:2 (wt/wt) PFQBDT-T2R$_2$:PC$_{61}$BM films (blue).

The most efficient BHJ cells exhibit interesting photovoltaic responses with PCEs of 5.7 % and 3.4%, respectively for as-cast 1:1 (wt/wt) PFQBDT-TR$_1$:PC$_{61}$BM and annealed 1:2 (wt/wt) PFQBDT-T2R$_2$:PC$_{61}$BM active blends. In particular, PFQBDT-TR$_1$ based solar cell exhibits J$_{SC}$ = 11.1 mA/cm^2, V$_{OC}$ = 0.84 V and FF = 61 %, while PFQBDT-T2R$_2$ based device shows J$_{SC}$ = 6.5 mA/cm^2, V$_{OC}$ = 0.96 V and FF = 54 %. By comparing the

resulting OPV characteristic, the main difference is represented by the J_{SC} and V_{OC} values, which exhibit an opposite trend passing from PFQBDT-TR$_1$ to PFQBDT-T2R$_2$.

The PFQBDT-TR$_1$ based solar cell based yields a current density of 11 mA/cm^2, almost the double of that of the corresponding PFQBDT-T2R$_2$ based device (6.5 mA/cm^2), in agreement with the different optical properties, both in pristine or blended films (Figure 2 and 5), and molecular packing of the polymer chains (Figure 3). The absorption spectra of the optimized active blends (Figure 5A) present a similar trend observed for pristine materials. Indeed, despite less pronounced differences, PFQBDT-TR$_1$:PC$_{61}$BM blend exhibits a broader and more defined absorption profile in the red portion of the spectrum, between 630 nm and 700 nm, suggesting enhanced $\pi-\pi$ interchain interactions, in agreement with improved charge transport properties, as supported by electrical and morphological investigations.

By comparing the average value of V_{OC} (V_{OC}^{av}) for each polymer:PC$_{61}$BM based solar cell, estimated from the open-circuit voltages observed at different D:A w/w ratios (Table 2), an increase in V_{OC}^{av} by ~ 0.15 V is observed passing from PFQBDT-TR$_1$ to PFQBDT-T2R$_2$. In particular, the best performing PFQBDT-TR$_1$ and PFQBDT-T2R$_2$ based solar cells exhibit a V_{OC} of 0.84 V and 0.96 V, respectively. This variation, despite the nearly identical electrochemically derived HOMO and LUMO energy levels (Table 1), could be ascribed to the effect of the side-chain architecture on the film-forming properties of the polymers, as supported by AFM images (Figure 6), likely influencing the exciton stabilization and dissociation, the D:A aggregation and interfacial energetics, all factors that are known to strongly affect the V_{OC}.[24, 10d] This, correlates well with our hypothesis that PFQBDT-TR$_1$, compared to PFQBDT-T2R$_2$, adopts a more planar conformation which promotes the generation of different and relatively more ordered and well-organized domains, in perfect agreement with the GIXD patterns, red-shifted absorption spectra and enhanced charge mobility, FF and J_{SC} values of PFQBDT-TR$_1$ based films. As mentioned, the hole mobility (estimated by space charge limited current (SCLC)[16] method, Figure S2) of optimized as-cast 1:1 (wt/wt) PFQBDT-TR$_1$:PC$_{61}$BM film resulted to be one order of magnitude higher compared to that of annealed 1:2 (wt/wt) PFQBDT-T2R$_2$:PC$_{61}$BM blend (2 x 10^{-4} and 4 x 10^{-5} cm^2 V^{-1} s^{-1}, respectively), in agreement with the higher J_{SC} and FF values (61% and 54%, respectively), which confirm a closer π-π stacking and ordering of PFQBDT-TR$_1$ polymer backbones. Note that, the relatively low mobility of PFQBDT-T2R$_2$ based films justifies the reduced thickness (~ 65 nm) required to optimize the photovoltaic responses of the resulting solar cells (Table 2).

The EQE spectra of the best performing PFQBDT-TR$_1$:PC$_{61}$BM and PFQBDT-T2R$_2$:PC$_{61}$BM based devices, as shown in Figure 5B, have spectral features which are consistent with the corresponding blend absorption spectra (Figure 5A), with a higher value for the PFQBDT-TR$_1$ based blend compared to the PFQBDT-T2R$_2$ based one. In particular, the EQE profiles of PFQBDT-TR$_1$:PC$_{61}$BM and PFQBDT-T2R$_2$:PC$_{61}$BM films showed maximum values of 65 % (at 600 nm) and 50 % (at 435 nm), respectively, corresponding to the relative absorption maxima of the blend. Convolution of these spectra with the AM1.5G solar spectrum gives calculated short circuit current density in good agreement, within a ~ 5 % experimental error, with that obtained from J–V measurements (Table 2 and Figure 4).

It is well known that the nanomorphology of the BHJ active layer plays an important role in determining the OPV performance. In order to gain a deeper understanding on how the side chain architecture of polymers PFQBDT-TR$_1$ and PFQBDT-T2R$_2$ affects the solar cell output parameters, we investigated the morphological differences of optimized PFQBDT-TR$_1$:PC$_{61}$BM and PFQBDT-T2R$_2$:PC$_{61}$BM blend films by tapping-mode AFM.
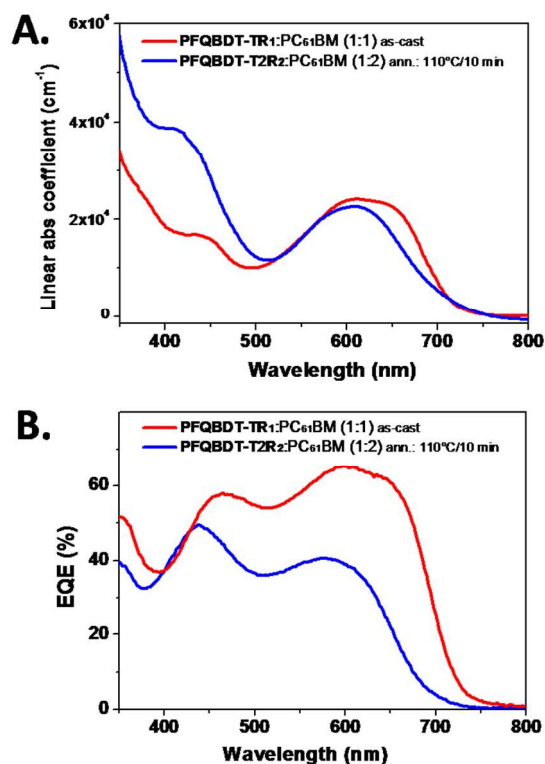

Figure 5. (A) UV−vis absorption spectra (normalized for the thickness of the films) and (B) EQE plots of: as-cast 1:1 (wt/wt) PFQBDT-TR$_1$: PC$_{61}$BM (red) and annealed 1:2 (wt/wt) PFQBDT-T2R$_2$: PC$_{61}$BM films (blue).

Figure 6 shows topographic images of the best performing BHJ cells based on as-cast 1:1 (wt/wt) PFQBDT-TR$_1$:PC$_{61}$BM and annealed 1:2 (wt/wt) PFQBDT-T2R$_2$:PC$_{61}$BM blends. The surface morphology of the resulting films are significantly different with morphological features that correlate well with the previous results. In particular, the topographic image of as-cast 1:1 (wt/wt) PFQBDT-TR$_1$:PC$_{61}$BM film is characterized by a well defined and structured surface (Root Mean Square, RMS, of ~ 5 nm) with reduced domain size suggesting the generation of an optimal phase separation between the BHJ components combined with the formation of more ordered and aggregated polymeric domains, as discussed above.

Diversely, despite the additional thermal treatment, the AFM image of annealed 1:2 (wt/wt) PFQBDT-T2R$_2$:PC$_{61}$BM exhibits a smooth and almost featureless surface (RMS of ~ 1 nm) with

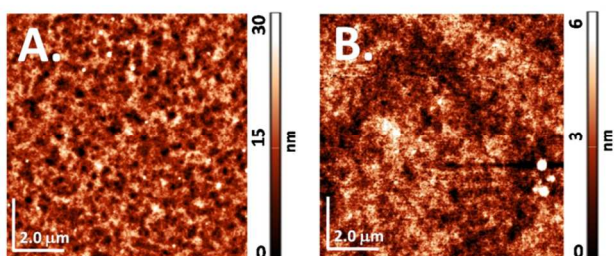quite large and poorly defined domains indicating a suboptimal phase segregation of the D:A blend.

Figure 6. Tapping mode AFM images (size: 10 μm × 10 μm) of optimized blends based on: A) as-cast 1:1 (wt/wt) PFQBDT-TR$_1$: PC$_{61}$BM (RMS = ~ 5 nm) and B) annealed 1:2 (wt/wt) PFQBDT-T2R$_2$: PC$_{61}$BM (RMS = ~ 1 nm).

Thus, poorly formed percolation pathways lead to limited charge transport and/or collection processes within the active blends, as confirmed by the low charge mobility, FF, and PCEs obtained from the corresponding BHJ films. This result correlates well with the above mentioned hypothesis on the twisting of PFQBDT-T2R$_2$ backbone which might partially hinder π-π interchain interactions, resulting in relatively more disordered and disaggregated domains.

Conclusions

In summary, two novel *p*-type quinoxaline-benzodithiophene copolymers, PFQBDT-TR$_1$ and PFQBDT-T2R$_2$, have been designed, synthesized, and characterized. We found that the alkyl substitution on the aromatic side group of the polymers significantly influences the *intra*- and *inter*-molecular interactions and thus the optical, morphological and electrical properties of the resulting films. In particular, polymer PFQBDT-TR$_1$, containing a single linear octyl (R$_1$, -C$_8$H$_{17}$) side chain on the thiophene rings, seems to adopt a more planar backbone conformation, compared to PFQBDT-T2R$_2$, which promotes the formation of aggregated and well-organized domains in blend films, in perfect agreement with the red-shifted absorption spectra, enhanced charge mobility, FF and J$_{SC}$ of the corresponding devices. In contrast, the two hexyl (R$_2$, -C$_6$H$_{13}$) side chains on thienyl groups of PFQBDT-T2R$_2$ can sterically hinder the adjacent quinoxaline unit inducing a backbone twisting which can be responsible for the different nanostructural order, blue-shifted absorption profiles and reduced electrical properties of the resulting thin films. Finally, while the PCE of the best performing PFQBDT-T2R$_2$ based device is 3.4 %, with J$_{SC}$ = 6.5 mA/cm^2, V$_{OC}$ = 0.96 V and FF = 54 %, the optimized PFQBDT-TR$_1$ based cell exhibits ~ 2 times improved PCE. In particular, the BHJ solar cell based on 1:1 (wt/wt) PFQBDT-TR$_1$:PC$_{61}$BM blend showed a PCE of 5.7 % with V$_{OC}$, J$_{SC}$, and FF of 0.84 V, 11.1 mA/cm^2, and 61%, respectively. Notably, all OPV devices were fabricated in ambient conditions by blade-coating technique.

Notes and references

$^{a)}$ *Consiglio Nazionale delle Ricerche (CNR), Istituto per lo Studio dei Materiali Nanostrutturati (ISMN), Via P. Gobetti, 101, 40129, Bologna, Italy.*

$^{b)}$ *Department of Chemical and Biological Engineering, Polymer Technology, Chalmers University of Technology, Goteborg, SE-412 96, Sweden. E-mail: antenehe@chalmers.se; mats.andersson@chalmers.se; Tel: +46 031 7723410; +46 031 7723401*

$^{c)}$ *Laboratory MIST E-R, Via P. Gobetti, 101, 40129, Bologna, Italy.*

$^{d)}$ *Consiglio Nazionale delle Ricerche (CNR), Istituto per la Microelettronica e Microsistemi (IMM), Via P. Gobetti, 101, 40129, Bologna.*

$^{e)}$ *Consiglio Nazionale delle Ricerche (CNR), Istituto per la Sintesi Organica e la Fotoreattività (ISOF), Via P. Gobetti, 101, 40129, Bologna, Italy. E-mail: mirko.seri@isof.cnr.it; Tel: +39 051 6399771.*

$^{f)}$ *Ian Wark Research Institute, University of South Australia, Mawson Lakes, South Australia 5095, Australia. E-mail: mats.andersson@unisa.edu.au; Tel:+61 8 8302 3106*

† Electronic Supplementary Information (ESI) available: Synthetic procedures for monomers and polymers, SWVs, optimization of device processing conditions, hole mobility measurements, ^{1}H and ^{13}CNMR spectra. See DOI: 10.1039/b000000x/

1. a) G. Li, R. Zhu and Y. Yang, *Nat. Photonics*, 2012, **6**, 153; b) F. C. Krebs, *Sol. Energy Mater. Sol. Cells*, 2009, **93**, 394; c) R. R. Søndergaard, M. Hosel and F. C. Krebs, *J. Polym. Sci., Part B: Polym. Phys.*, 2013, **51**, 16.

2. G. Yu, J. Gao, J. C. Hummelen, F. Wudl and A. J. Heeger, *Science*, 1995, **270**, 1789.

3. L. Dou, J. You, Z. Hong, Z. Xu, G. Li, R.A. Street and Y. Yang, *Adv. Mater.,* 2013, **25**, 6642.

4. a) H. Yip and A. K.-Y. Yen, *Energy Environ. Sci.*, 2012, **5**, 5994; b) Y.-J. Cheng, S.-H. Yang and C.-S. Hsu, *Chem. Rev.,* 2009, **109**, 5868; c) M. Seri, M. Bolognesi, Z. Chen, S. Lu, W. Koopman, A. Facchetti and M. Muccini, *Macromolecules*, 2013, **46**, 6419; d) W. Zhuang, M. Bolognesi, M. Seri, P. Henriksson, D. Gedefaw, R. Kroon, M. Jarvid, A. Lundin, E. Wang, M. Muccini and M. R. Andersson, *Macromolecules*, 2013, **46**, 8488.

5. a) M. T. Dang, L. Hirsch, G. Wantz and J. D. Wuest, *Chem. Rev.*, 2013, **113**, 3734; b) C. R. McNeill, *Energy Environ. Sci.*, 2012, **5**, 5653.

6. Z. C. He, C. M. Zhong, S. J. Su, M. Xu, H. B. Wu and Y. Cao, *Nat. Photonics*, 2012, **6**, 591; b) S.-H. Liao, H.-J.

Jhuo, Y.-S. Cheng and S.-A. Chen, *Adv. Mater.*, 2013, **25**, 4766; c) J. Jo, J.-R. Pouliot, D. Wynands, S. D. Collins, J. Y. Kim, T. L. Nguyen, H. Y. Woo, Y. Sun, M. Leclerc and A. J. Heeger, *Adv. Mater.*, 2013, **25**, 4783; d) M. Bolognesi, M. Tessarolo, T. Posati, M. Nocchetti, V. Benfenati, M. Seri, G. Ruani and M. Muccini, *Org. Photon. Photovolt.*, 2013, **1**, 1; e) N. Zhou, X. Guo, R. Ponce Ortiz, S. Li, S. Zhang, R. P. H. Chang, A. Facchetti, T. J. Marks, *Adv. Mater.*, 2012, **24**, 2242; f) L. Motiei, Y. Yao, J. Choudhury, He Yan, T. J. Marks, M. E. van der Boom, A. Facchetti, *J. Am. Chem. Soc.* 2010, **132**, 12528.

7. a) F. C. Krebs, N. Espinosa, M. Hösel, R. R. Søndergaard and M. Jørgensen, *Adv. Mater.*, 2014, **26**, 29; b) N. Espinosa, M. Hosel, M. Jørgensen, F. C. Krebs, *Energy Environ. Sci.*, 2014, **7**, 855.

8. a) Y. Liang and L. Yu, *Acc. Chem. Res.*, 2010, 43, 1227; b) A. Facchetti, *Chem. Mater.*, 2011, **23**, 733.

9. a) D. M. de Leeuw, M. M. J. Simenon, A. R. Brown and R. E. F. Einerhand, *Synth. Met.* 1997, **87**, 53; b) M. C. Scharber, D. Mülbacher, M. Koppe, P. Denk, C. Waldauf, A. J. Heeger and C. J. Brabec, *Adv. Mater.*, 2006, **18**, 789; c) C. J. Brabec, A. Cravino, D. Meissner, N. S. Sariciftci, T. Fromherz, M. T. Rispens, L. Sanchez and J. C. Hummelen, *Adv. Funct. Mater.*, 2001, **11**, 374.

10. a) H. Y. Chen, J. H. Hou, S. Q. Zhang, Y. Y. Liang, G. W. Yang, Y. Yang, L. P. Yu, Y. Wu and G. Li, *Nat. Photonics*, 2009, **3**, 649; b) H. X. Zhou, L. Q. Yang, A. C. Stuart, S. C. Price, S. B. Liu and W. You, *Angew. Chem. Int. Ed.*, 2011, **50**, 2995; c) I.Osaka, M. Saito, T. Koganezawa and K. Takimiya, *Adv. Mater.*, 2013, **26**, 331; d) Y. Wang, Y. Liu, S. Chen, R. Peng, Z. Ge, *Chem. Mater.*, 2013, **25**, 3196; e) A. Abbotto, M. Seri, M. S. Dangate, F. De Angelis, N. Manfredi, E. Mosconi, M. Bolognesi, R. Ruffo, M. M. Salamone, M. Muccini, *J. Polym. Sci., Part A: Polym. Chem.* 2012, **50**, 2829.

11. a) J. Min, Z.-G. Zhang, S. Zhang and Y. Li, *Chem. Mater.*, 2012, **24**, 3247; b) J. Hou, Z. Tan, Y. Yan, Y. He, C. Yang and Y. Li, *J. Am. Chem. Soc.*, 2006, **128**, 4911; c) Y. Li and Y. Zou, *Adv. Mater.*, 2008, **20**, 2952; d) L. Huo, S. Zhang, X. Guo, F. Xu, Y. Li and J. Hou, *Angew. Chem. Int. Ed.*, 2011, **50**, 9697; e) Y. Huang, X. Guo, F. Liu, L. Huo, Y. Chen, T. P. Russell, C. C. Han, Y. Li and J. Hou, *Adv. Mater.*, 2012, **24**, 3383; f) F. Zhang, V. Roznyatovskiy, F.-R. F. Fan, V. Lynch, J. L. Sessler and A. J. Bard, *J. Phys. Chem. C*, 2011, **115**, 2592; g) D. Gedefaw, M. Tessarolo, W. Zhuang, R. Kroon, E. Wang, M. Bolognesi, M. Seri, M. Muccini and M. R. Andersson, *Polym. Chem.*, 2014, **5**, 2083; h) R. Gutzler, D. F. Perepichka, *J. Am. Chem. Soc.* 2013, **135**, 16585.

12. M. Bolognesi, D. Gedefaw, D. Dang, P. Henriksson, W. Zhuang, M. Tessarolo, E. Wang, M. Muccini, M. Seri and M. R. Andersson, *RSC Adv.*, 2013, **3**, 24543.

13. H.-C. Chen, Y.-H. Chen, C.-C. Liu, Y.-C. Chien, S.-W. Chouand and P.-T. Chou, *Chem. Mater.*, 2012, **24**, 4766.

14. a) Z.-G. Zhang, J. Min, S. Zhang, J. Zhang, M. Zhang and Y. Li, *Chem. Commun.*, 2011, **47**, 9474; b) Y. Deng, Y. Chen, J. Liu, L. Liu, H. Tian, Z. Xie, Y. Geng and F. Wang, *ACS Appl. Mater. Interfaces*, 2013, **5**, 5741; c) L. Yang, H. Zhou and W. You, *J. Phys. Chem. C*, 2010, **114**, 16793; d) B. Wang, J. Zhang, H. L. Tam, B. Wu, W. Zhang, M. S. Chan, F. Pan, G. Yu, F. Zhu and M. S. Wong, *Polym. Chem*, 2014, **5**, 836; e) V. S. Gevaerts, E. M. Herzig, M. Kirkus, K. H. Hendriks, M. M. Wienk, J. Perlich, P.M. Buschbaum, R. A. J. Janssen, *Chem. Mater.* 2014, **26**, 916.

15. a) V. V. Pavlishchuk and A. W. Addison, *Inorg. Chim. Acta*, 2000, **298**, 97; b) A. J. Bard and L. R. Faulkner, *Electrochemical Methods: Fundamentals and Applications*, 2nd edn., John Wiley & Sons, New York, 2001.

16. a) D. S. Chung, D. H. Lee, C. Yang, K. Hong, C. E. Park, J. W. Park and S. K. Kwon, *Appl. Phys. Lett.*, 2008, **93**, 033303; b) P. W. M. Blom, M. J. M. de Jong and J. J. M. Vleggaar, *Appl. Phys. Lett.*, 1996, **68**, 3308.

17. X. Wang, Y. Sun, S. Chen, X. Guo, M. Zhang, X. Li, Y. Li and H. Wang, *Macromolecules*, 2012, **45**, 1208.

18. a) I. Osaka, M. Saito, T. Koganezawa and K. Takimiya, *Adv. Mater.*, 2014, **26**, 331; b) J. Min, Y. N. Luponosov, A. Gerl, M. S. Polinskaya, S. M. Peregudova, P.V. Dmitryakov, A. V. Bakirov, M. A. Shcherbina, S. N. Chvalun, S. Grigorian, N. Kaush-Busies, S. A. Ponomarenko, T. Ameri and C. J. Brabec, *Adv. Energy Mater.*, 2013, DOI: 10.1002/aenm.201301234; c) Y. Liu, X. Wan, F. Wang, J. Zhou, G. Long, J. Tian, J. You, Y. Yang, and Y. Chen, *Adv. Energy Mater.* 2011, **1**, 771.

19. a) Y. Huang, X. Guo, F. Liu, L. Huo, Y. Chen, T. P. Russell, C. C. Han, Y. Li, J. Hou, *Adv. Mater.*, 2012, **24**, 3383; b) C. Piliego, T. W. Holcombe, J. D. Douglas, C. H. Woo, P. M. Beaujuge, J. M. J. Fréchet, *J. Am. Chem. Soc.*, 2010, **132**, 7595; c) H.-C. Chen, Y.-H. Chen, C.-H. Liu, Y.-H. Hsu, Y.-C. Chien, W.-T. Chuang, C.-Y. Cheng, C.-L. Liu, S.-W. Chou, S.-H. Tung, P.-T. Chou, *Polym. Chem.*, 2013, **4**, 3411.

20. L. Huo, J. Hou, S. Zhang, H. Y. Chen and Y. Yang, *Angew.Chem. Int. Ed.*, 2010, **49**, 1500.

21. Y. He, G. Zhao, B. Peng and Y. Li, *Adv. Funct. Mater.*, 2010, **20**, 3383.

22. D. J. Servaites, M. A. Ratner and T. J. Marks, *Energy Environ. Sci.*, 2011, **4**, 4410.

23. a) A. Moliton and J.-M. Nunzi, *Polym. Int.*, 2005, **55**, 583; b) B. Kippelen and J.-L. Brédas, *Energy Environ. Sci.*, 2009, **2**, 251.

24. a) M. D. Perez, C. Borek, S. R. Forrest, M. E. Thompson, *J. Am. Chem. Soc.* 2009, **131**, 9281; b) J. Liu, Y. Shi, Y. Yang, *Adv. Funct. Mater.* 2001, **11**, 420; c) E. Wang, J. Bergqvist, K. Vandewal, Z. Ma, L. Hou, A. Lundin, S. Himmelberger, A. Salleo, C.Müller, O. Inganäs, F.Zhang and M. R. Andersson, *Adv. Energy Mater.*, 2013, **3**, 806; d) K. Vandewal, K. Tvingstedt, A. Gadisa, O. Inganäs, J. V. Manca, *Nature Mater.*, 2009, **8**, 904; e) R. Noriega, J. Rivnay, K. Vandewal, F. P. V. Koch, N. Stingelin, P. Smith, M. F. Toney, A. Salleo, *Nature Mater.*, 2013, **12**, 1038; f) K. Vandewal, S. Himmelberger, A. Salleo, *Macromolecules*, 2013, **46**, 6379.

Structural tuning of Quinoxaline-Benzodithiophene copolymers *via* alkyl side chain manipulation: Synthesis, Characterization and Photovoltaic Properties.

Marta Tessarolo, Desta Gedefaw, Margherita Bolognesi, Fabiola Liscio, Patrik Henriksson, Wenliu Zhuang, Silvia Milita, Michele Muccini, Ergang Wang, Mirko Seri and Mats R. Andersson

Graphical abstract.